

# Tocopherol Activity Correlates with Its Location in a Membrane: A New Perspective on the Antioxidant Vitamin E

Drew Marquardt,<sup>†</sup> Justin A. Williams,<sup>‡</sup> Norbert Kučerka,<sup>¶</sup> Jeffrey Atkinson,<sup>§</sup> Stephen R. Wassall,<sup>‡</sup> John Katsaras,<sup>||,⊥,†,¶</sup> and Thad A. Harroun<sup>\*,†</sup>

<sup>†</sup>Department of Physics, Brock University, St. Catharines, Ontario L2S 3A1, Canada

<sup>‡</sup>Department of Physics, Indiana University–Purdue University Indianapolis, Indianapolis, Indiana 46202, United States

<sup>¶</sup>Canadian Neutron Beam Centre, National Research Council, Chalk River, Ontario K0J 1J0, Canada,

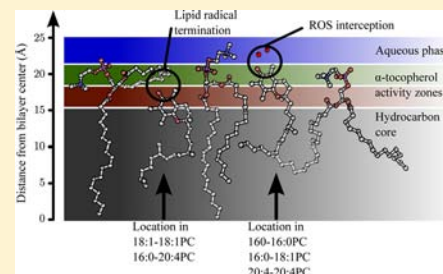
<sup>§</sup>Department of Chemistry, Brock University, St. Catharines, Ontario L2S 3A1, Canada

<sup>||</sup>Oak Ridge National Laboratory, Oak Ridge, Tennessee 37831-6393, United States

<sup>⊥</sup>Joint Institute for Neutron Sciences, Oak Ridge, Tennessee 37831, United States

## Supporting Information

**ABSTRACT:** We show evidence of an antioxidant mechanism for vitamin E which correlates strongly with its physical location in a model lipid bilayer. These data address the overlooked problem of the physical distance between the vitamin's reducing hydrogen and lipid acyl chain radicals. Our combined data from neutron diffraction, NMR, and UV spectroscopy experiments all suggest that reduction of reactive oxygen species and lipid radicals occurs specifically at the membrane's hydrophobic–hydrophilic interface. The latter is possible when the acyl chain “snorkels” to the interface from the hydrocarbon matrix. Moreover, not all model lipids are equal in this regard, as indicated by the small differences in vitamin's location. The present result is a clear example of the importance of lipid diversity in controlling the dynamic structural properties of biological membranes. Importantly, our results suggest that measurements of aToc oxidation kinetics, and its products, should be revisited by taking into consideration the physical properties of the membrane in which the vitamin resides.



## INTRODUCTION

Despite its being discovered over 80 years ago, the biological role of vitamin E remains a subject of much controversy.<sup>1,2</sup> Vitamin E deficiency can lead to several health disorders including infertility<sup>3</sup> and neuromuscular dysfunction,<sup>4</sup> but molecular descriptions of how these effects arise are for the most part, nonexistent. Regardless of its well-known antioxidant properties as a stand-alone molecule, recent assertions have implied that vitamin E may not perform the same function in living systems. The lack of a clear antioxidant health benefit from vitamin supplements, and its naturally low *in vivo* concentrations have led to the idea that vitamin E's presence may have more to do with cell signaling, apoptosis, protein activity, and even gene regulation than any direct first line of defense regarding lipid peroxidation.<sup>4–9</sup>

Vitamin E is comprised of two families of compounds, which differ in side-chain saturation. Tocopherols have a fully saturated side chain, while the side chain of tocotrienols contains three double bonds.<sup>10</sup> The four most common chromanol ring homologues differ in methylation at two locations on the chromanol ring. Although all 8 vitamin E family members share a number of similarities,  $\alpha$ -tocopherol (aToc, Figure 1) is the only one that is retained by the human body, and used by the only known vitamin E receptor, namely aTTP ( $\alpha$ -tocopherol transport protein), which is responsible for

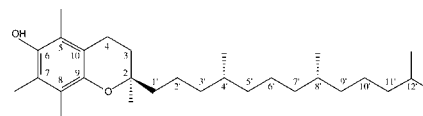


Figure 1.  $\alpha$ -tocopherol.

regulating the physiological concentrations of tocopherols and tocotrienols.<sup>11</sup>

aToc is found either in lipid rafts<sup>12,13</sup> or, as we have previously suggested, in polyunsaturated phospholipid-rich domains.<sup>14</sup> Its nominal upright orientation in a membrane has its chromanol ring pointing toward the lipid headgroup, while its phytyl tail resides closer to the bilayer center.<sup>15–17</sup> aToc has not only been implicated in intercepting free radicals diffusing into the membrane from the aqueous phase, near the lipid–water interface,<sup>15,18–20</sup> but also in terminating lipid peroxy radical oxidation chain reactions deep in the membrane.<sup>17,21–23</sup> Surprisingly, the discrepancy between these two modes of action has received little notice, even though the two sources of radicals are not in close proximity to each other.

Received: December 28, 2012

Published: April 12, 2013

A simpler biophysical justification for aToc's location within a membrane may be found when comparing it to cholesterol, which unlike aToc exerts its primary function as a structural component, rather than a molecule associated with a specific biochemical reaction. Cholesterol's lipid-ordering properties are driven by steric interactions, where it orders the lipid hydrocarbon chains, thus minimizing their free energy. In highly disordered bilayers made up of polyunsaturated fatty acid chains, cholesterol has been found to sequester at the bilayer center, a location vastly different from its nominal upright orientation, where it associates with sphingomyelin.<sup>24,25</sup> The hopping of cholesterol between membrane leaflets in response to membrane composition is one way that cholesterol is able to modulate the structural properties of membranes, and by extension, the function of membrane-integral proteins.<sup>26</sup> The lack of an identifiable receptor for any aToc-mediated signal leads us to treat it similarly to cholesterol; i.e., aToc responds to the presence of oxidation-susceptible lipids primarily through steric interactions, but in such a manner that it may be able to protect them from damaging free radicals.

Using different physical characterization techniques (i.e., neutron diffraction, NMR and UV spectroscopy) we report on aToc's location in model membranes, and how its location can affect its antioxidant abilities. We propose that aToc's location in a membrane is well fixed through steric interactions of its phytol tail and chromanol headgroup, and the type of lipid bilayer in which it resides in. Details are given regarding its depth, dynamics, and molecular orientation in hetero- and homo-unsaturated phosphatidylcholine lipid bilayers. Taken together, these results clearly show that aToc's location and antioxidant activity correlate precisely with the depth of its sacrificial hydroxyl (on the chromanol ring) within the different lipid membranes studied.

## RESULTS

**Structure and Hydration of Membranes Containing aToc.** Oriented membrane multilayers were adsorbed to silicon single crystal substrates and hydrated in a 94% relative humidity environment. When exposed to a monochromatic neutron beam, quasi-Bragg peaks were observed which corresponded to the lamellar repeat spacings ( $d \approx 50\text{--}55 \text{ \AA}$ ) for the different membranes. Fourier transformation of the neutron scattering data with the appropriate phases resulted in the 1D scattering length density (SLD) profile of the membrane. (The SLD is the amplitude of the neutron de Broglie wave scattered from the sample nuclei, and is analogous to the electron density of X-ray crystallography.)

The dashed black lines in Figure 2 show the 1D SLD profile of lipid samples containing 10 mol% of aToc, and the solid black lines are same composition samples, but with deuterium-labeled aToc-5d3. The figure shows bilayers with increasing degree of chain unsaturation, from top-to-bottom; 16:0-16:0PC, 16:0-18:1PC, 18:1-18:1PC, 16:0-20:4PC, and 20:4-20:4PC, respectively.

A unit cell contains one bilayer and the origin of the abscissa corresponds to the bilayer center. The interlayer water is located at the edges of the unit cell (blue line, see below). Maxima (black lines) at  $\sim \pm 15\text{--}20 \text{ \AA}$  roughly indicate the position of the glycerol-ester backbone. (X-ray scattering experiments are most sensitive to the high electron density of the phosphate.) The distance between these peaks roughly defines the bilayer hydrophobic thickness (Table 1),<sup>27</sup> and the dip in SLD at the bilayer center is the result of disordered (i.e.,

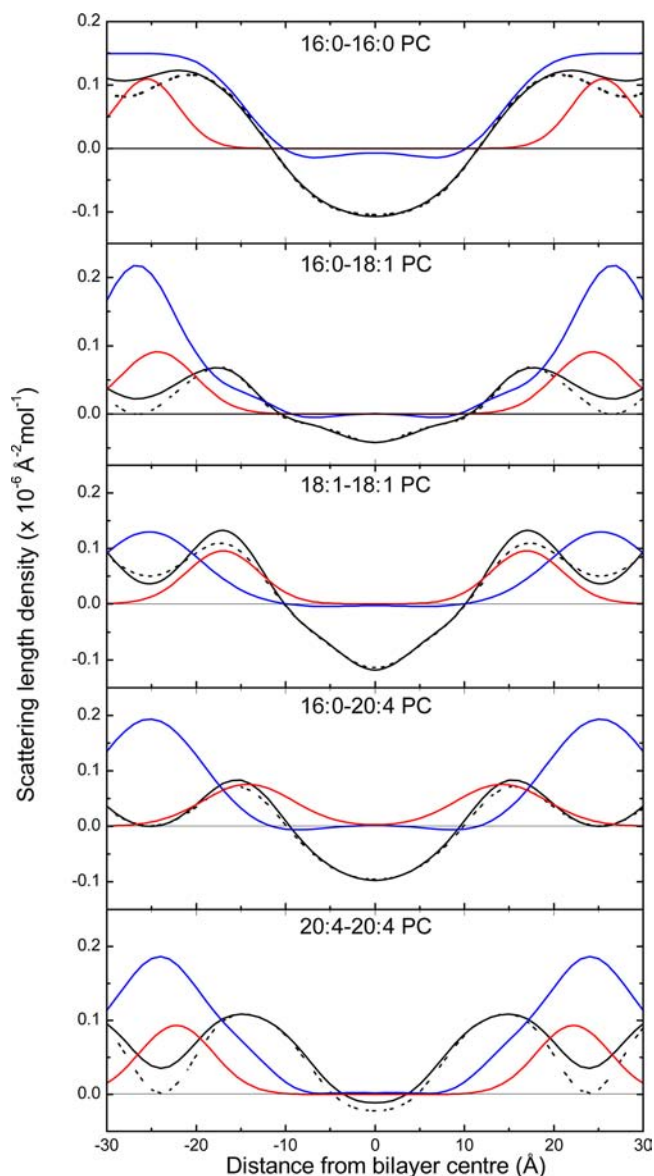


**Figure 2.** Neutron scattering length data (analogous to X-ray electron density) of aToc-5d3 in various liquid crystalline phosphatidylcholine membranes. Solid black lines: lipid and labeled aToc at 8%  $^2\text{H}_2\text{O}$ . Dashed black lines: lipid and proteated aToc, at 8%  $^2\text{H}_2\text{O}$ . Red lines: Difference between solid and dashed black lines, resulting in the mass distribution of aToc's C5-methyl label. Blue lines: Difference between the 8%  $^2\text{H}_2\text{O}$  data and the same sample at 40%  $^2\text{H}_2\text{O}$ , showing the mass distribution of the interlayer water.

increased motion) terminal methyl groups, and where the greatest density of hydrogen occurs. At a similar level of hydration, our unit-cell dimensions for 16:0-16:0PC bilayers agree with previous X-ray measurements.<sup>28</sup>

From the data we also determined the penetration of water into the membrane by exploiting the contrast between light water ( $^1\text{H}_2\text{O}$ ) and heavy water ( $^2\text{H}_2\text{O}$ ). This is based on the fact that deuterium nuclei have a positive scattering length, while in the case of hydrogen, it is negative—selective substitution of deuterium for hydrogen allows for the location of deuterium atoms to be easily located through subtraction of the two 1D SLDs. The solid black lines of Figure 2 are data that were taken at a water composition of 8%  $^2\text{H}_2\text{O}$ , rendering water essentially “invisible” to neutrons. Effectively then, at 8%  $^2\text{H}_2\text{O}$

**Table 1. Measured (Unit Cell) and Calculated (Other) Structural Parameters for  $\alpha$ -[5- $^2\text{H}_3$ ]Tocopherol (aToc-5d3) in Different Phosphatidylcholine Membranes<sup>a</sup>**

PC lipid	unit cell size	bilayer thickness	label position	label 1/e width	water peak	water 1/e width
16:0–16:0	56.09	35.72(7)	25.5(3)	3.77(4)	28.2(3)	7.43(8)
16:0–18:1	53.19	35.72(7)	24.2(3)	4.22(5)	26.6(3)	7.71(9)
18:1–18:1	50.10	35.4(1)	17.0(2)	4.00(4)	26.8(3)	11.0(1)
16:0–20:4	50.25	31.7(1)	14.2(2)	5.57(6)	25.1(3)	7.67(8)
20:4–20:4	47.80	28.31(6)	22.2(2)	4.03(4)	24.0(2)	9.8(1)

<sup>a</sup>aToc's position is relative to the bilayer center, and the range that it occupies is determined from the widths, 1/e, of Gaussian fits to the data. Units are angstroms.

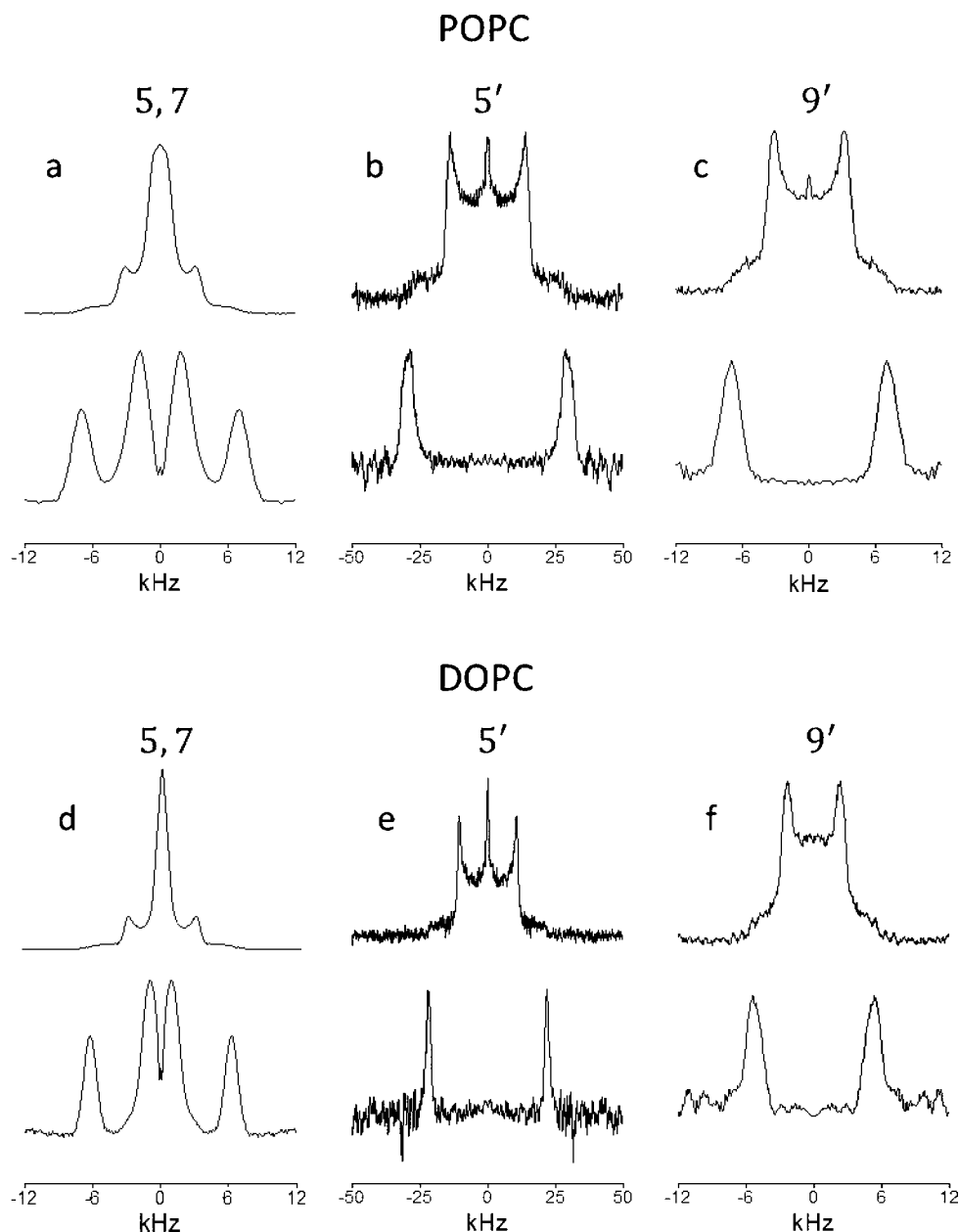


**Figure 3.**  $\alpha$ -Tocopherol spectra:  $^2\text{H}$  NMR spectra for 50 wt% 16:0–18:1PC (POPC) dispersions in 50 mM Tris buffer (pH 7.5) containing 10 mol % aToc-5,7d6 (a), aToc-5'd2 (b), and aToc-9'd2 (c) (top panel), and 18:1–18:1PC (DOPC) bilayers containing 10 mol% aToc-5,7d6 (d), aToc-5'd2 (e) and aToc-9'd2 (f) (bottom panel) at 30 °C. In each case, the spectrum obtained by conventional FFT and its corresponding FFT depaked spectrum (below) are shown. The experiments were conducted on resonance and the out-of-phase channel was zeroed, thus improving the signal-to-noise of 2.5 of the spectra that were reflected about their central (resonant) frequency.

the 1D SLD is entirely the result of scattering from only the lipids and aToc (i.e., only membrane is “visible”). The solid

blue line is determined by subtracting the 8%  $^2\text{H}_2\text{O}$  data (black curve) from the same chemical composition membrane at 70%

$^2\text{H}_2\text{O}$  (not shown), and represents the distribution of water across the membrane.

Modeled as a Gaussian distribution, the amount of interlayer water typically reaches a  $1/e$  value near, or outside the peak of the 8%  $^2\text{H}_2\text{O}$  SLD, i.e., the lipid's glycerol backbone. The exception are 16:0–16:0PC bilayers at 50 °C, where the water seems to penetrate below the hydrogen belt (region of the glycerol ester with its CO hydrogen bond acceptors, capable of lipid–lipid H-bonding via a suitable donor such as cholesterol or water) of the backbone. The increased polar environment surrounding the headgroup of this lipid will be important later when discussing previously published data.

The effect of aToc on acyl chain structure, shown in Figure 2, is to alter structural features normally associated with pure saturated and mono-unsaturated lipids. For example, in pure 18:1–18:1PC lipid bilayers the C9 double bond can often be observed as a plateau in 1D electron density and SLD profiles,<sup>29</sup> a feature that is no longer present in Figure 2. In fact, the SLD profiles in Figure 2 are similar to PUFA bilayers, where few acyl chains are distinguishable.<sup>25,30</sup> It therefore seems that aToc has a significant disordering effect on the lipid acyl chains of the different bilayers studied.

**Location of the  $\alpha$ -Tocopherol in PC Bilayers.** Neutron diffraction experiments similar to the ones described were also carried-out with C5-methyl  $^2\text{H}_3$ -labeled aToc (aToc-5d3). Difference SLD profiles reveal the time and sample averaged mass distribution of the aToc chromanol C5-methyl (i.e., the average location). In practice, the black SLD curves are not subtracted from each other in real-space; instead a single Gaussian distribution is assumed for the distribution of the label, and its Fourier transform is fitted to the corrected data in reciprocal space.<sup>25,30</sup> In real space, such as the data in Figure 2, such subtractions are subject to fluctuations as a result of having only four or five terms (quasi-Bragg reflections) sampling the Fourier series; thus we show the best-fit Gaussians in their entirety as red curves in Figure 2. The distribution is well described by a single Gaussian, whose center is at 15 and 25 Å from the middle of the bilayer, and each of width between 3 and 5 Å. The positions and widths of the peaks corresponding to the aToc chromanol C5-methyl are recorded in Table 1.

From these data it seems that aToc is found in two locations within the membrane. In 16:0–16:0PC, 16:0–18:1PC, and 20:4–20:4PC bilayers the C5-methyl label is well above the hydrophobic/hydrophilic interface, with the chromanol group residing in among the lipid choline headgroups. In contrast, in 18:1–18:1PC and 16:0–20:4PC bilayers the C5-methyl label is located closer to the lipid's glycerol backbone, near the hydrogen belt.

The different results in aToc depth between bilayers with common *sn*-2 chains (e.g., between 16:0–18:1PC and 18:1–18:1PC, and between 16:0–20:4PC and the 20:4–20:4PC), is surprising. This result was reconfirmed with solid-state  $^2\text{H}$  NMR using deuterium-labeled analogues of aToc incorporated into 16:0–18:1PC and 18:1–18:1PC membranes, whereby the molecular organization of aToc in its “high” (16:0–18:1PC) and “low” (18:1–18:1PC) membrane positions could be compared. Figure 3 shows  $^2\text{H}$  NMR spectra for aqueous multilamellar dispersions of 16:0–18:1PC and 18:1–18:1PC bilayers containing 10 mol% aToc-5,7d6, aToc-5'd2, and aToc-9'd2. Conventional FFT and depacked FFT spectra are shown. Conventional spectra of aToc analogues labeled in their phytyl side chain (aToc-5'd2 and aToc-9'd2) are a superposition of doublets produced by membranes at all orientations

relative to the magnetic field (Figure 3b,c (upper) and e,f (upper))

The two peaks separated by

$$\Delta\nu = \frac{3}{4} \left( \frac{e^2 q Q}{h} \right) |S_{\text{CD}}| \quad (1)$$

dominate the powder pattern, where  $(e'qQ/h) = 168$  kHz is the static quadrupolar coupling constant, and  $S_{\text{CD}}$  is the order parameter describing the angular motion of the C– $^2\text{H}$  bond with respect to the bilayer normal. The powder pattern becomes a doublet in the FFT depacked spectra (Figure 3b,c (lower) and e,f (lower)), which are equivalent to the spectrum for a planar membrane and possess enhanced spectral resolution, with a splitting

$$\Delta\nu(\theta) = \frac{3}{2} \left( \frac{e^2 q Q}{h} \right) |S_{\text{CD}}| P_2(\cos \theta) \quad (2)$$

where  $\theta = 0$  is the angle between the bilayer normal and the magnetic field, and  $P_2(\cos \theta)$  is the second order Legendre polynomial. Because there are two sites of deuteration, the conventional spectrum for the analogue labeled in the chromanol headgroup (aToc-5,7d6) is a superposition of two powder patterns (Figure 3a,d (upper)). The outer spectral component with two well-defined peaks is assigned to the 7 and 5 positions, according to a published work.<sup>16</sup> The two peaks which are not resolved for the inner powder pattern are the result of line broadening, which is on the order of the quadrupolar splitting. Inner and outer doublets are, however, resolved in the FFT depacked spectra (Figure 3a,d (lower)). Order parameters calculated using eq 2 from the depacked spectra of 16:0–18:1PC and 18:1–18:1PC bilayers containing aToc-5,7d6, aToc-5'd2, and aToc-9'd2, are listed in Table 2.

**Table 2. Order Parameters  $S_{\text{CD}}$  for Deuterated Analogues of aToc Incorporated at 10 mol% into 16:0–18:1PC and 18:1–18:1PC Bilayers at 30 °C**

deuterium position	$S_{\text{CD}}$	
	16:0–18:1PC	18:1–18:1PC
5	0.015	0.008
7	0.055	0.050
5'	0.234	0.174
9'	0.057	0.042

The values obtained for  $S_{\text{CD}}$  are small ( $\leq 0.055$ ), and comparisons of the 5- and 7-labeled positions of aToc in both 16:0–18:1PC and 18:1–18:1PC bilayers (Figure 2) suggest a similar orientation for the chromanol headgroup in the two membranes. It should be borne in mind, however, that these small order parameters do not imply that the nominally rigid headgroup is disordered, since geometric factors as well as angular motion contribute to the order parameter. Indeed, previously reported quadrupolar splitting data from deuterated analogues of aToc in egg PC bilayers were best fit when angular fluctuations of the chromanol group were assigned a molecular order parameter of  $S_{\text{mol}} = 0.53$ .<sup>16</sup>

In contrast to the order parameters for the 5 and 7 positions on the chromanol group, order parameters that are markedly larger in 16:0–18:1PC, compared to 18:1–18:1PC bilayers, were measured for the 5' and 9' positions of aToc's side chain (Table 2). Consistent with the neutron scattering data, we

attribute these differences to aToc's location namely that, compared to 18:1–18:1PC, aToc sits higher in 16:0–18:1PC bilayers. Support for this interpretation is garnered from the smoothed order parameter profiles plotted in Figure 4, which

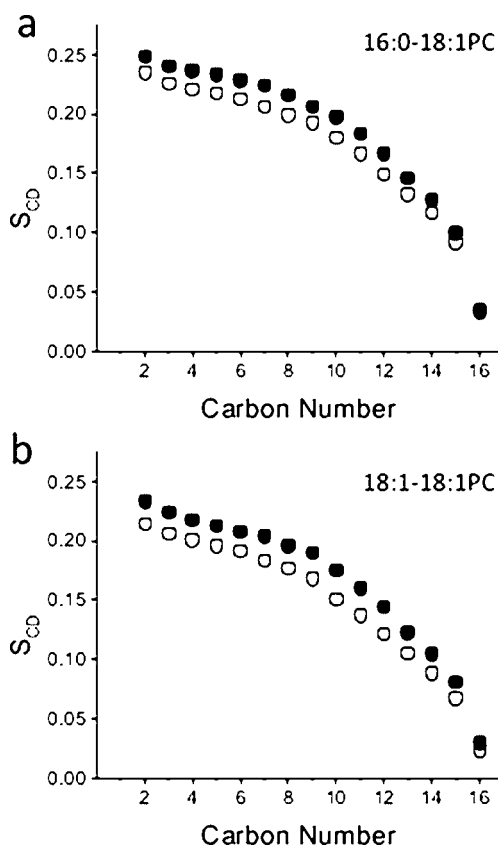


**Figure 4.** Smoothed order parameter profiles of 5 mol% PA-d31 in (a) 16:0–18:1PC and (b) 18:1–18:1PC bilayers with (●) and without (○) 10 mol% aToc at 30 °C.

represent molecular organization within the host membranes. The order parameter profiles were constructed from the FFT depaked  $^2\text{H}$  NMR spectra of 16:0–18:1PC and 18:1–18:1PC membranes containing 5 mol% [ $^2\text{H}_{31}$ ]palmitic acid (PA-d31), with and without 10 mol% aToc (shown in Supporting Information). As can be seen, for both 16:0–18:1PC (Figure 4a) and 18:1–18:1PC membranes (Figure 4b) the order varies slowly in the portion of the chain closer to the membrane's surface (C2–9), and decreases more rapidly toward the middle of the bilayer (C10–16)—such a profile is characteristic of PC membranes in the liquid crystalline phase.<sup>31</sup> The order parameter's profile is not altered by the addition of aToc but is simply increased throughout its range. Compared to 18:1–18:1PC (5%), this increase is more pronounced in 16:0–18:1PC (10%) bilayers, and comparable to what has previously been seen in a saturated PC membrane.<sup>32</sup> The higher order parameters observed in 16:0–18:1PC (Figure 4a) bilayers are consistent with the order parameter profiles determined from two membrane systems with PA-d31 included.

Significantly, the difference in order parameter for the 5' position on aToc's phytol chain ( $\Delta S = 0.060$ ) between the two systems greatly exceeds that detected at any position along the intercalated fatty acid chain ( $\Delta S \leq 0.022$ ). From this we infer that in 16:0–18:1PC bilayers aToc sits higher so that the motion of its 5' position is constrained because its location is such that

it penetrates into the plateau region of elevated order in the surrounding membrane. This is in contrast to the 18:1–18:1PC bilayer, where aToc sits deeper in the membrane, and beyond the plateau region where the disorder in the surrounding membrane decreases precipitously as one approaches the bilayer center. In the case of Toc-9'd2, the smaller order parameters and reduction in differential between 16:0–18:1PC and 18:1–18:1PC bilayers (Figure 2) can then be understood in terms of aToc's 9' position on its side chain residing in the more disordered region of both membranes. In short, the NMR results are found to be consistent with data from neutron scattering.

#### Tocopherol Depth Correlates with Lipid Oxidation.

We tested the notion that aToc's location correlates with its position in the bilayer by examining lipid oxidation initiated in the water region, outside the bilayer (water-borne Fenton's reagent chemistry for generating hydroxyl radicals):



or within the membrane's hydrocarbon core (hydrophobic 2,2'-azobis(2,4-dimethylvaleronitrile), i.e., AMVN chemistry for generating alkyl radicals from thermolysis<sup>33</sup>):



Both reactions were initiated in an anaerobic environment, so that reactions involving peroxy radicals ( $\text{OOH}^\bullet$ ) were suppressed, although it is possible in Fenton reagents to generate small amounts of oxygen. Our hypothesis, therefore, is that aToc residing deeper in the membrane should interact with both AMVN radicals and diffusing reactive oxygen species (ROS) from the water, whereas aToc closer to the lipid/water interface should have less interaction with oxidation reactions taking place within the bilayer's acyl chains (hydrophobic region).

We monitored the time evolution of UV absorption,  $A$ , from lipid vesicles undergoing oxidation by free radical generation, with and without 10 mol% of aToc (shown in Figures 5 and 6; complete time-series data are included in the Supporting Information). It has been argued that the oxidation susceptibility of lipids varies linearly, or even exponentially, as a function of double bonds in the hydrocarbon chains (degree of unsaturation).<sup>34</sup> In the case of lipid bilayers with extremely low oxidation susceptibilities (i.e., 16:0–16:0PC, Figure 5, and 18:1–18:1PC, Figure 6), they initially show low absorption at wavelengths above 200 nm. However, in the case of medium to high oxidation susceptible lipids (16:0–20:4PC, Figure 5, 20:4–20:4PC, Figure 6), despite the extreme care that we took in handling them, small amounts of oxidized lipids were detected, as noted by the small rise in  $A$  around 230 nm. The presence of aToc is noted by the shoulder in the UV spectra at 300 nm, and a maximum value of  $A \geq 3$  at 220 nm.<sup>22</sup> It should be noted that the amount of oxidizing initiator was kept below half the amount of aToc so that aToc could not be quickly used up, thus enabling easier detection of the reaction products.

UV spectra of lipid oxidation are dominated by the strong absorption from the conjugated dienes produced in the presence of hydroxyl and carbon-centered radicals. It is not necessary that we account for the exact species of radicals, as their presence is noted by an overall increase in  $A$ , especially in

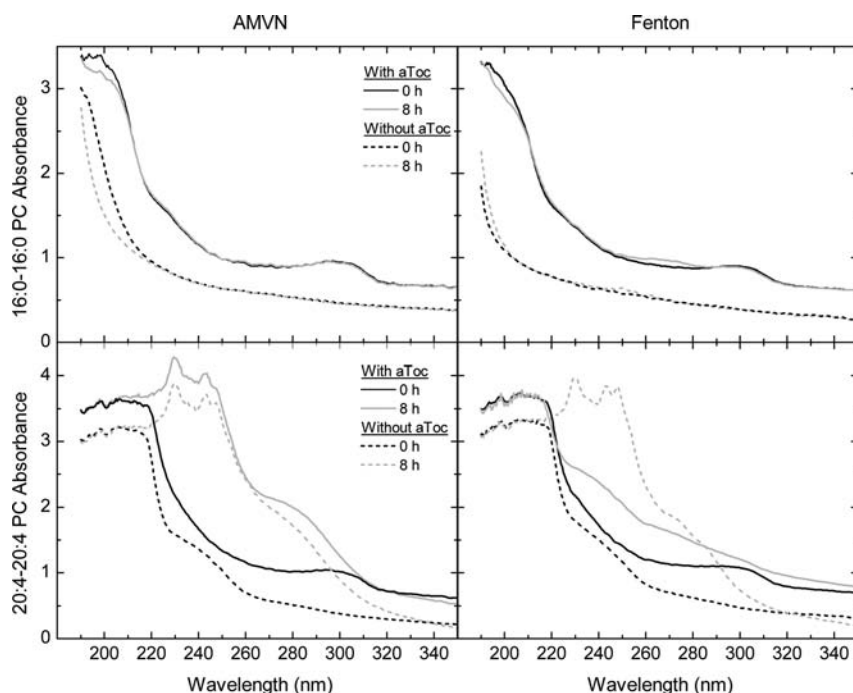


**Figure 5.** UV absorption of 16:0–16:0PC (top panels) and 20:4–20:4PC bilayers (bottom panels) for oxidation at time  $t = 0$  (black lines) and  $t = 8$  h (gray lines) using the Fenton reagent (right panels) or AMVN (left panels). Experiments were performed both with (solid lines) and without (dashed lines) aToc.

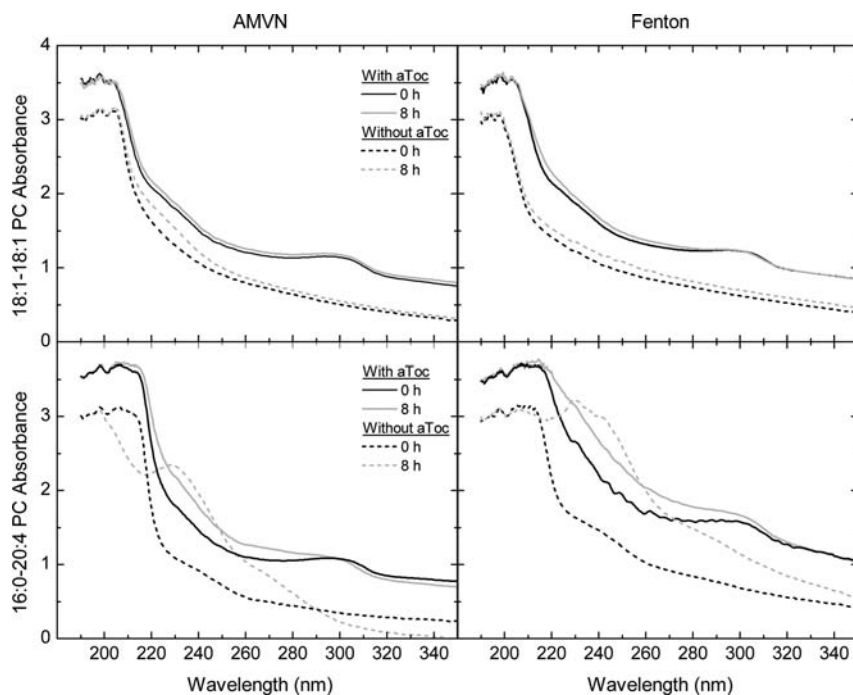


**Figure 6.** UV absorption of 18:1–18:1PC (top panels) and 16:0–20:4PC bilayers (bottom panels) for oxidation at time  $t = 0$  (black lines) and  $t = 8$  h (gray lines) using the Fenton reagent (right panels) or AMVN (left panels). Experiments were performed both in the presence (solid lines) and in the absence (dashed lines) of aToc.

the region of 230–260 nm, and  $A \geq 3$  for wavelengths  $< 230$  nm. In the case of the lipid least susceptible to oxidation (16:0–16:0PC), no oxidation products were detected even after 8 h of exposure to Fenton peroxides or AMVN radicals (Figure 5), although AMVN breakdown products did result in a small rise in the  $A$  baseline. However, the presence of quinone products from tocopherol oxidation was indicated by the

shoulder starting at 260 nm, and peaking near 269 nm, but only in the case of the Fenton reaction.<sup>35</sup> The location of the chromanol ring near the lipid/water interface (as determined from neutron scattering data) is far less accessible to the hydrophobic AMVN radicals—although in excess amounts of AMVN, well above the concentrations used in the present

studies, it has been shown that aToc oxidation can occur over a period of about 10 h.<sup>36</sup>

In contrast, the lipid most susceptible to oxidation (20:4–20:4PC) experiences significant amounts of degradation regardless of the chemistry used to induce oxidation (i.e., thermal breakdown (data not shown), AMVN, or Fenton chemistry) (Figure 5). The rate of oxidation is greater in the case of Fenton chemistry, presumably because lipid radicals can terminate more often with nearby AMVN breakdown products i.e., the AMVN-initiated chain reaction then proceeds more slowly. Nevertheless, the near total oxidation breakdown of the unsaturated hydrocarbon chains must take place through a chain reaction. Keeping in mind the near anaerobic state of the AMVN samples, this chain reaction must occur through carbon-centered, non-hydroxyl lipid radicals. The oxidized lipid (having lost only one hydrogen atom) will rearrange itself to form the conjugated diene, but the carbon radical can only be quenched either by another carbon radical or by abstracting an H atom from another PUFA.

As expected, from the data in Figure 5 it is clear that aToc notably impedes the oxidation process in 20:4–20:4PC bilayers. However, it offers the most protection against ROS diffusing from bulk water, and even after 8 h had prevented significant oxidation damage by Fenton chemistry from taking place. In contrast, aToc could only delay, but could not prevent, AMVN oxidation. Thus aToc located near the membrane/water interface is capable of intercepting ROS diffusion from reaching the unsaturated bonds of the hydrocarbon chains, but cannot terminate a chain reaction taking place deep in the membrane—unless a chain's *trans*–*gauche* isomerization causes the acyl chain to “snorkel” at least to the level of the headgroup's  $\alpha$  or  $\beta$  carbons (*vide infra*).

Even lipids with moderate susceptibility to oxidation (18:1–18:1PC, 16:0–20:4PC, Figure 5) are consistent with this notion of oxidative damage. The oxidation of 16:0–20:4PC proceeds similarly to that of 20:4–20:4PC, but with smaller *A* values, the result of fewer lipid radicals. However, aToc eliminates nearly all oxidation in both AMVN and Fenton initiated reactions. Here is where the lower location of aToc in the bilayer plays a key role. By residing closer to the glycerol backbone aToc has much greater access to snorkeling acyl-chains, thus efficiently terminating oxidation reactions. For 18:1–18:1PC, the results from this moderately stable lipid are comparable to 16:0–16:0PC. Notice, however, that UV absorption of quinone reaction products from the reaction with ROS are only seen in 16:0–16:0PC bilayers, where aToc's hydroxyl group resides in the higher position. aToc resides lower in 18:1–18:1PC, and is less accessible to ROS. As mentioned, no significant amounts of quinone were detected in our limited quantity AMVN reactions.

## DISCUSSION

Our data show that aToc can reside in two different locations in not so dissimilar bilayers. These locations affect aToc's ability to reduce the different radical species, and enable it to intercept diffusing ROS or terminate lipid radical chain reactions. The balance between these two modes of action is achieved by the steric packing of the lipids making up the membrane. (Since all lipids in this study contain the same zwitterionic PC headgroup, the various aToc-PC headgroup interactions should be the same.)

Our neutron diffraction data show that the average mass distribution of aToc's hydroxyl is firmly located high in the

bilayer, i.e., at the lipid/water interface and not within the hydrocarbon matrix. There is no ambiguity associated with this result, and was directly obtained without the use of bulky spin labels or probes. Experiments making use of labels and probes tend to place the chromanol nearest the quenching probe that has maximum effectiveness, e.g., refs 22, 23, and 37. The quenching probes have been assumed to reside deeper in the bilayer than actual fact, and their position has been inferred from the notion that probe position along the stearic acid carrier molecule correlates roughly with the probe's depth in the bilayer.

Interestingly, we have found that aToc's location does not change systematically with the degree of hydrocarbon unsaturation, whether an overall degree of unsaturation, or on a specific chain. In fact, such an observation was previously made by Urano et al., where <sup>13</sup>C T1 relaxation measurements at 50 °C found that there was little difference in the motion of aToc's isoprenoid side-chains in 16:0–16:0PC liposomes and rat liver lecithin rich in polyunsaturated arachidonic acid (20:4) at the *sn*-2 position, but a significant decrease in segmental motion was observed for the of the same *sn*-2 position chains in egg yolk lecithin, a lipid mixture rich in linoleic (18:2) and oleic (18:1) acids.<sup>38</sup> The similarity of aToc's isoprenoid side-chain motion in palmitic acid and arachidonic acid, and how it differs in the presence of linoleic and oleic acids, is borne-out by our neutron data in Figure 2.

There have been a few inferences regarding aToc's location in a membrane, which were based on NMR measurements of its chromanol moiety. T2 relaxation of CF<sub>3</sub>-labeled aToc at the chromanol 5-methyl—the same location as in our studies—showed significantly reduced molecular motion in 16:0–16:0PC liposomes.<sup>19</sup> This was interpreted to mean that the chromanol moiety was tightly packed in the vicinity of the lipid/water interface. Other <sup>13</sup>C NMR studies also observed the reduced molecular motion of aToc's chromanol moiety, and suggested that aToc's hydroxyl group is hydrogen bonded to some acceptor in the headgroup,<sup>39</sup> although it has been suggested that such bonding is negligible, and that sterically driven entropic forces dominate.<sup>40</sup> Using T1 and T2 relaxation measurements of <sup>13</sup>C, Srivastava et al. also noted reduced chromanol motion, but suggested that the ring is located practically in the aqueous phase, arguing that any hydrogen bonding with the lipids should take place with the phosphate oxygen, in excellent agreement with our data.<sup>41</sup>

We note one other NMR measurement intended to locate aToc in bilayers, namely that by Afri et al. who used an indirect technique that correlates <sup>13</sup>C NMR chemical shift to the solvent's polarity.<sup>20</sup> Based on their interpretation of Reichardt's *E<sub>T</sub>* dye experiments, they located the C5 and C7-methyls of aToc residing near the lipid/water interface.<sup>20</sup> However, the hydrophilic–hydrophobic interface they used to interpret their data seems much too narrow to us, and based on the amount of water that we determined which penetrates the lipid bilayer (Figure 2), the assigned *E<sub>T</sub>* values around the lipid headgroup were most likely underestimated.

**$\alpha$ -Tocopherol Acts Only at the Membrane Surface.** Lipid auto-oxidation is dominated by hydrogen abstraction from bis-allylic methylene followed by the creation of free radicals (LH→L<sup>•</sup>), and less so from the loss of hydrogen from monoallylic or alkyl carbons, or even direct reaction with superoxide oxygen.<sup>34</sup> In the presence of oxygen, lipid peroxyl radicals (LOO<sup>•</sup>) are more likely to be formed and to propagate oxidation damage than simpler carbon-centered radicals (L<sup>•</sup>).<sup>18</sup>

The inhibition of oxidation by aToc seems to be in part due to the termination of both the lipid peroxy radical and lipid carbon-centered radical chain reactions. This has been confirmed by the many adduct products that have been previously identified from allylic chain oxidation.<sup>42,43</sup> Based on our data, we suggest that this can only occur when the PUFA chain “snorkels” to the high level of the chromanol, and should in fact be the rate limiting step.

It seems that the seemingly large distance between the chromanol hydroxyl and the chain methylenes has been recognized as a potential problem, but with little attention paid to it. The idea that termination of lipid radical propagation is rate limited has been expressed by others, but based on less than reliable information regarding the depth of aToc's hydroxyl, and not a chain conformation mechanism.<sup>18,35</sup> Early on, Fukuzawa expressed doubts regarding the ability of secondary organic radicals to reach and oxidize aToc.<sup>35,44</sup> Moreover, and without any direct evidence, Barclay et al. postulated that the trapping of a polar peroxy radical must take place near the polar headgroup region, and that lipid peroxy radicals diffuse to the membrane's surface region in order to terminate with the antioxidant.<sup>45</sup> This explanation, however, cannot account for nonpolar lipid radical termination, since the implication is that hydrophobic forces drive the diffusion of the polar peroxy radicals to the membrane surface. Furthermore neither of the above-mentioned studies could indicate, with any degree of certainty, the location of this activity.

Although counterintuitive, it is well known that polyunsaturated acyl chains spend a significant fraction of their time interacting with the choline headgroups. This is a greatly under appreciated fact, even by those who recognize its existence.<sup>19</sup> The NMR cross-relaxation rates from the choline  $\gamma$ -methyl resonance to resonances at the methyl end of hydrocarbon chains are small, but important.<sup>46–48</sup> The much lower energy barrier for rotation about the C–C bonds of methylene groups in polyunsaturated chains allow for sub-nanosecond conformational transitions, producing a higher degree of chain disorder, and allowing for even greater cross-relaxation between headgroup and chain resonances.<sup>46</sup> In fact, docosahexaenoic acid (22:6) chains have been shown to explore their entire conformational space within a mere 50 ns.<sup>49</sup>

Initial evidence that oxidation termination takes place at the membrane surface comes from the identification of isomers formed from the oxidation of 16:0–20:4PC bilayers.<sup>50</sup> Hydroxy peroxide occurs most frequently at carbons 5 and 15 of the hydrocarbon chain, or the innermost and outermost positions when in heterogeneous liposomes (40% and 33% of the time, respectively). Addition of aToc distributes the OH among the 5, 8, 9, 11, 12, and 15 carbons equally, meaning that hydrogen donation between the 7, 10, and 13 bis-allylic carbons is practically equal.<sup>50</sup> Since our results do not indicate that aToc spends any time at the different depths, it must therefore be that the polar peroxy radicals rise to meet the aToc hydroxy with equal frequency. Note, that no preference with respect to carbon position was seen in the NMR cross-relaxation rates with the choline  $\gamma$ -methyl resonance,<sup>46</sup> indicating that “snorkling” chain conformation is not “U-shaped” but a random and highly disordered process.

Further support for the snorkling process comes from our experiments with AMVN, which were carried out in reduced O<sub>2</sub> conditions. In these cases, the lipid free-radical was carbon-centered (L $\cdot$ ), not a peroxy radical (LOO $\cdot$ ), and thus would not diffuse by hydrophobic forces to the membrane surface.

Instead, termination relied upon highly disordered hydrocarbon chains to bring the radicals to the surface.

## CONCLUSION

Determining the location of aToc's hydroxyl in the membrane is important in understanding the chemistry of lipid oxidation, since microenvironments within the bilayer could alter the physical location of oxidants, antioxidants, and oxidation substrates. In the physical chemistry of oil-in-water emulsions, such as those important in the cosmetic and food industries, this has been termed the “antioxidant polar paradox”, which postulates that nonpolar antioxidants are more effective in oil-in-water emulsions than polar antioxidants.<sup>51,52</sup> In considering the more complex biological environment of the plasma membrane, why does aToc locate its hydroxyl group so near the hydrophilic interface?

Healthy cells require the presence of oxidants which are created through various natural enzymatic and nonenzymatic pathways. A survey of the most common oxidants reveals that in the case of PUFA lipids the deleterious species originate in the cell's inter- and intracellular fluid.<sup>53</sup> By far, the two most prevalent free radicals *in vivo* are the superoxide anion (O<sub>2</sub> $\cdot^-$ ) and nitric oxide (NO $\cdot$ ).<sup>54–56</sup> Even free-radical-producing enzymatic processes predominantly take place in cytosolic and peripheral membrane proteins.<sup>57,58</sup> Important exceptions to this are found in the mitochondrial membrane, where cellular respiration occurs,<sup>55–58</sup> and specifically in the PUFA metabolism enzyme, lipoxygenase.<sup>59</sup> Early experiments indicated that up to 3% of electrons in the electron transport chain of cellular respiration “leak” out from the transport chain to create ROS superoxide radical anions.<sup>56</sup> Cadenas and Sies, in 1998, agreed that most superoxide formation occurs within the mitochondria of a cell.<sup>60</sup> Nonenzymatic sources of free radicals are metal ions in the inter- and intracellular fluid, and those formed from ionizing radiation. Fenton chemistry can proceed with a variety of transition metals, most commonly Fe(II) which is found *in vivo*,<sup>56,58</sup> but can also include other metals such as copper, cobalt, and chromium.<sup>54</sup> Thus, for the plasma membrane to be compromised, virtually all of the ROS must approach the cell membrane from the cytosol rather than from hydrophobic media (the center of a lipid bilayer).

Therefore, it seems obvious that lipophilic antioxidants such as aToc would have more affinity for the hydrophobic–water interface and, thus would inhibit lipid oxidation more efficiently from that location. We have presented neutron diffraction, NMR and UV spectroscopic data regarding the location and function of aToc in membranes. The data all indicate that aToc's antioxidant activity takes place exclusively at the membrane's surface, either through the interception of diffusing ROS species, or the termination of lipid radicals, which as a result of their high conformational disorder routinely rise to the level of the tocopherol hydroxyl group. It is clear from the data that aToc does not explore the hydrophobic center of the lipid bilayer in order to terminate lipid peroxy radicals, rather it is firmly anchored through steric forces at the lipid/water interface, with its phytyl tail residing among the lipid acyl chains (Figure 7). This result also has implications with regard to aToc's interaction with free radicals *in vivo*.

For advocates of aToc as an antioxidant, aToc's particular location in a membrane allows for its hydroxyl group to be positioned at the lipid/water interface, providing easy access to polar soluble reducing agents, such as ascorbate, which rapidly recycles the tocopheroxyl radical back to aToc. The limited

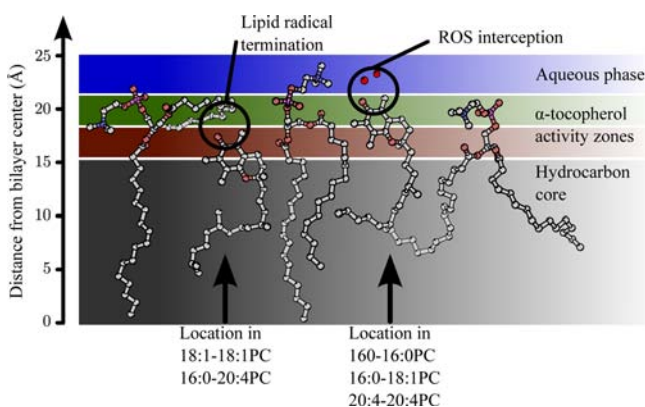


**Figure 7.** Schematic of aToc in a model lipid membrane as determined by neutron diffraction. The zones of aToc antioxidant action are confined to the region of the glycerol ester and above, extending practically to the aqueous phase. Although aToc can either terminate a lipid radical or intercept diffusing ROS, its different locations within bilayers correlate well with its primary activity. Lipid models are of 16:0–18:1PC taken from ref 61.

evidence in humans that aToc functions as a fat soluble antioxidant in response to oxidative stress indicates that aToc does not prevent radical formation in the cytosol, or even in the initial oxidation of fatty acyl chains, but that aToc does stop lipid peroxide chain reactions and reduces the presence of radicals that diffuse into the bilayer.<sup>9</sup> By using different acyl chain PC bilayers we have demonstrated that aToc positions itself into specific locations through steric interactions, and it is these specific membrane locations that determine how aToc exercises its antioxidant capability.

To continue to test this theory, we will in the future consider different lipid bilayers, including those with different head-groups and sphingolipids. Furthermore, the role of steric interactions can be further elucidated with pentamethyl chromane, or tail-less aToc. In addition, the observed similarity of aToc to cholesterol with regards to lipid order in different phases indicates that cholesterol may modulate aToc function. Presently, we have only studied aToc's vertical positioning in lipid bilayers, however, the diversity of lipids found in eukaryote cells implies that aToc's lateral diffusion within a membrane will also be affected by the different lipid species.

## EXPERIMENTAL PROCEDURES

**Materials.** Phosphatidylcholine lipids were purchased from Avanti Polar Lipids (Alabaster, AL), and after experimentation were evaluated by TLC. The lipids studied were of the form 1-acyl-2-acyl-*sn*-glycero-3-phosphatidylcholine, specifically dipalmitoyl (16:0–16:0PC), palmitoyl-oleoyl (16:0–18:1PC), dioleoyl (18:1–18:1 PC), diarachidonoyl (20:4–20:4PC), and palmitoyl-arachidonoyl (16:0–20:4PC).

$\alpha$ -[5-<sup>2</sup>H<sub>3</sub>]Tocopherol (aToc-5d3) was prepared following published procedures.<sup>62,63</sup> Briefly,  $\gamma$ -tocopherol was aminomethylated by heating with morpholine and deuterated formaldehyde. The crude product was then reduced using sodium cyanoborodeuteride (NaCNBD<sub>3</sub>). After purification by silica gel column chromatography, the deuterium incorporation at the 5-C<sup>2</sup>H<sub>3</sub> group was judged to be >96.5% by mass spectroscopy.

$\alpha$ -[5,7-<sup>2</sup>H<sub>6</sub>]Tocopherol (aToc-5,7d6),  $\alpha$ -[5-<sup>2</sup>H<sub>2</sub>]tocopherol (aToc-5'd2), and  $\alpha$ -[9-<sup>2</sup>H<sub>2</sub>]tocopherol (aToc-9'd2) were previously synthesized,<sup>16</sup> while D- $\alpha$ -tocopherol (aToc) was purchased from Cole-Parmer (Vernon Hills, IL). Cambridge Isotope Laboratories (Andover, MA) supplied <sup>2</sup>H<sub>3</sub>1-palmitic acid (PA-d31) and deuterium-depleted water.

**Neutron Diffraction.** The methods of sample preparation and neutron diffraction follow those described previously.<sup>24,26</sup> All preparations of aligned multilayer samples were carried out in a nitrogen environment. A total of 12 mg of phospholipid with 10 mol%  $\alpha$ -tocopherol was co-dissolved in chloroform or chloroform–trifluoroethanol (3:1). The solution was deposited onto a silicon single crystal substrate, and the solvent evaporated, while gently rocking the sample. This procedure produces well aligned lamellar samples in a reproducible manner. Samples were then placed in a vacuum for ~2 h to remove traces of the solvent, and subsequently placed in airtight sample cells. Samples were hydrated at fixed humidity using a saturated salt solution of KNO<sub>3</sub> (94% RH) with 0, 8, 16, and/or 40 mol% <sup>2</sup>H<sub>2</sub>O, and kept at room temperature during initial equilibration. Experiments were conducted in the liquid crystalline phase at 25.0 ± 0.5 °C for all the lipids except for 16:0–16:0PC, for which the temperature was 50 °C.

Neutron diffraction data were taken on the N5 and D3 spectrometers located at the Canadian Neutron Beam Center (CNBC, Chalk River, Ontario, Canada), and the AND/R NG-1 instrument at the NIST Center for Neutron Research (NCNR, Gaithersburg, Maryland). Neutron wavelengths were selected using single crystal monochromators, and were 2.37 Å at the CNBC and 5.0 Å at the NCNR. At both facilities, filters were used to eliminate higher order (i.e.,  $\lambda/2$ , etc.) reflections. Typically, 4–8 quasi-Bragg peaks were recorded, and the reconstructed unit cells have a nominal resolution of 9–11 Å. Bragg peaks were monitored for stability over time, indicating full equilibration at a given hydration and temperature. Furthermore, *d*-spacing were ensured to be reproducible between the separately prepared labeled and unlabeled samples. No specimen showed multiple Bragg peaks, which might have indicated inhomogeneity of the specimen across the substrate.

Data correction and reconstruction of the bilayer profile proceeded as outlined in a previous paper.<sup>26</sup> The 1D SLD profile  $\rho(z)$  was constructed with the cosine transform of the measured form factors  $F_h$ . The difference between labeled and unlabeled data was calculated from the difference in the measured form factors;  $F_h = F_h^{\text{labeled}} - F_h^{\text{unlabeled}}$ . Data were placed on an absolute scale by calculating the total SLD of the unit cell, in units of Å<sup>-2</sup> mol<sup>-1</sup>, and for every sample condition.

**<sup>2</sup>H NMR Spectroscopy.** Samples were aqueous multilamellar dispersions of 50 wt% lipid in 50 mM Tris buffer (pH 7.5). Phospholipid and 10 mol% deuterated analogue of aToc were co-dissolved in chloroform, and the organic solvent was removed under a stream of argon followed by vacuum pumping. The dried lipid was thoroughly mixed with buffer and the pH adjusted. After 1–3 lyophilizations with deuterium-depleted water to reduce naturally abundant <sup>2</sup>H<sub>2</sub>O, samples were transferred to a 5 mm NMR tube. Essentially the same procedure was employed preparing samples comprised of phospholipid with PA-d31 (5 mol%) in the absence and presence of aToc.

NMR spectra were acquired at 30 °C on a home-built spectrometer operating at 7.05 T employing a phase alternated quadrupolar echo sequence.<sup>64,65</sup> Spectral parameters were as follows: 90° pulse width, ~3  $\mu$ s; separation between pulses  $\tau$ , 50–100  $\mu$ s; delay between pulse sequences, 0.25–1.5 s; sweep width, ±50–100 kHz; data set, 2K; and 100 000–400 000 transients.

**UV/Visible Spectroscopy.** For pure lipid samples, 1 mg of lipid was hydrated with degassed ultrapure water. Samples containing 10 mol%  $\alpha$ -tocopherol and/or 0.1 mol% AMVN were co-dissolved in chloroform, which was then removed by vacuum (1 h) and then hydrated with degassed ultrapure water. Lipid suspensions were then extruded using a filter populated with 200 nm diameter pores, and loaded into quartz cuvettes. For external oxidation conditions, Fenton reagents (FeSO<sub>4</sub> and H<sub>2</sub>O<sub>2</sub>) were added to the lipid dispersion immediately prior to data collection. The oxidation was monitored with an Ultraspec 2100 pro UV/visible spectrophotometer. For internal oxidation conditions, samples contained AMVN and were held at 50 °C, regardless of lipid type, to ensure a sufficient rate of radical production—the plasma half-life of RRR-tocopherol is 45–60 h.<sup>9</sup> In all cases, the lipids were studied in the liquid crystalline phase.

## ■ ASSOCIATED CONTENT

## ● Supporting Information

Additional experimental details; structure factors for the neutron SLD profiles; NMR data for the PA-d31 experiments; full time course of the UV spectra; and NMR and mass spectroscopy analysis of the labeled aToc. This material is available free of charge via the Internet at <http://pubs.acs.org>.

## ■ AUTHOR INFORMATION

## Corresponding Author

thad.harroun@brocku.ca

## Notes

The authors declare no competing financial interest.

## ■ ACKNOWLEDGMENTS

We acknowledge the support of the National Institute of Standards and Technology, U.S. Department of Commerce, in providing the AND/R neutron research facilities used in this work. This project was supported by National Science and Engineering Research Council of Canada (NSERC). The authors are grateful to the Canadian Neutron Beam Centre (Chalk River) for supporting neutron diffraction measurements. T.A.H. gratefully acknowledges support from the Research Corporation through the Cottrell College Science Award. J.K. is supported by the Laboratory Directed Research and Development Program of Oak Ridge National Laboratory, managed by UT-Battelle, LLC, for the U.S. Department of Energy (DOE). Support for J.K. from the Scientific User Facilities Division of the Office of Basic Energy Sciences is also acknowledged.

## ■ REFERENCES

- Brigelius-Flohe, R.; Davies, K. J. A. *Free Radical Biol. Med.* **2007**, *43*, 2–3.
- Brigelius-Flohe, R.; Galli, F. *Mol. Nutr. Food Res.* **2010**, *54*, 583–587.
- Evans, H. M.; Bishop, K. S. *Science* **1922**, *56*, 650–651.
- Gohil, K.; Vash, V. T.; Cross, C. E. *Mol. Nutr. Food Res.* **2010**, *54*, 693–709.
- Zingg, J.-M. *Mol. Aspects Med.* **2007**, *28*, 481–506.
- Traber, M. G. *Annu. Rev. Nutr.* **2007**, *27*, 347–362.
- Azzi, A. *Free Radical Biol. Med.* **2007**, *43*, 16–21.
- Traber, M. G. *Mol. Nutr. Food Res.* **2010**, *54*, 661–668.
- Traber, M. G.; Stevens, J. F. *Free Radical Biol. Med.* **2011**, *51*, 1000–1013.
- DellaPenna, D. J. *Plant Physiol.* **2005**, *162*, 729–737.
- Traber, M. G.; Atkinson, J. *Free Radical Biol. Med.* **2007**, *43*, 4–15.
- Royer, M.-C.; Lemaire-Ewing, S.; Desrumaux, C.; Monier, S.; de Barros, J.-P.; Athias, A.; Néel, D.; Lagrost, L. *J. Biol. Chem.* **2009**, *284*, 15826–15834.
- Lemaire-Ewing, S.; Desrumaux, C.; Néel, D.; Lagrost, L. *Mol. Nutr. Food Res.* **2010**, *54*, 631–640.
- Atkinson, J.; Harroun, T.; Wassall, S. R.; Stillwell, W.; Katsaras, J. *Mol. Nutr. Food Res.* **2010**, *54*, 641–651.
- Perly, B.; Smith, I. C. P.; Hughes, L.; Burton, G. W.; Ingold, K. U. *Biochim. Biophys. Acta* **1985**, *819*, 131–155.
- Ekiel, I. H.; Hughes, L.; Burton, G. W.; Jovall, P. A.; Ingold, K. U.; Smith, I. C. P. *Biochemistry* **1988**, *27*, 1432–1440.
- Takahashi, M.; Tsuchiya, J.; Niki, E. *J. Am. Chem. Soc.* **1989**, *111*, 6350–6353.
- Buettner, G. R. *Arch. Biochem. Biophys.* **1993**, *300*, 535–543.
- Urano, S.; Matsuo, M.; Sakanaka, T.; Uemura, I.; Koyama, M.; Kumadaki, I.; Fukuzawa, K. *Arch. Biochem. Biophys.* **1993**, *303*, 10–14.
- Afri, M.; Ehrenberg, B.; Talmon, Y.; Schmidt, J.; Cohen, Y.; Frimer, A. A. *Chem. Phys. Lipids* **2004**, *131*, 107–121.
- Kagan, V. E.; Quinn, P. J. *Eur. J. Biochem.* **1988**, *171*, 661–667.
- Aranda, F. J.; Coutinho, A.; Berberan-Santos, M. N.; Prieto, M. J. E.; Gómez-Fernández, J. C. *Biochim. Biophys. Acta* **1989**, *985*, 26–32.
- Fukuzawa, K. *J. Nutr. Sci. Vitaminol.* **2008**, *54*, 273–285.
- Harroun, T. A.; Katsaras, J.; Wassall, S. R. *Biochemistry* **2006**, *45*, 1227–1233.
- Harroun, T. A.; Katsaras, J.; Wassall, S. R. *Biochemistry* **2008**, *47*, 7090–7096.
- Kucerka, N.; Marquardt, D.; Harroun, T. A.; Nieh, M.-P.; Wassall, S. R.; Katsaras, J. *J. Am. Chem. Soc.* **2009**, *131*, 16358–16359.
- Kucerka, N.; Nieh, M.-P.; Katsaras, J. *Biochim. Biophys. Acta* **2011**, *1808*, 2761–2771.
- Quinn, P. J. *Eur. J. Biochem.* **1995**, *233*, 916–925.
- Darkes, M. J. M.; Bradshaw, J. P. *Acta Crystallogr.* **2000**, *D56*, 48–54.
- Mihailescu, M.; Gawrisch, K. *Biophys. J.: Biophys. Lett.* **2006**, *90*, L04–L06.
- Pauls, K. P.; MacKay, A. L.; Bloom, M. *Biochemistry* **1983**, *22*, 6101–6109.
- Wassall, S. R.; Thewalt, J. L.; Wong, L.; Gorrissen, H.; Cushley, R. J. *Biochemistry* **1986**, *25*, 319–326.
- Niki, E. *Methods Enzymol.* **1990**, *186*, 100–108.
- Wagner, B. A.; Buettner, G. R.; Burns, C. P. *Biochemistry* **1994**, *33*, 4449–4453.
- Fukuzawa, K.; Gebicki, J. M. *Arch. Biochem. Biophys.* **1983**, *226*, 242–251.
- Liebler, D. C.; Kaysen, K. L.; Burr, J. A. *Chem. Res. Toxicol.* **1991**, *4*, 89–93.
- Fukuzawa, K.; Ikebata, W.; Shibata, A.; Kumadaki, I.; Sakanaka, T.; Urano, S. *Chem. Phys. Lipids* **1992**, *63*, 69–75.
- Urano, S.; Iida, M.; Otani, I.; Matsuo, M. *Biochem. Biophys. Res. Commun.* **1987**, *146*, 1413–1418.
- Salgado, J.; Villalain, J.; Gómez-Fernández, J. C. *Eur. Biophys. J.* **1993**, *22*, 151–155.
- Qin, S.-S.; Yu, Z.-W. *J. Phys. Chem. B* **2009**, *113*, 16537–16546.
- Srivastava, S.; Phadke, R. S.; Govil, G.; Rao, C. N. R. *Biochim. Biophys. Acta* **1983**, *734*, 353–362.
- Yamauchi, R.; Yagi, Y.; Kato, K. *Biochim. Biophys. Acta* **1994**, *1212*, 43–49.
- Yamauchi, R. Addition Products of  $\alpha$ -tocopherol with Lipid-Derived Free Radicals. *Vitamins and Hormones*; Elsevier: Amsterdam, 2007; Vol. 76, Chapter 11, pp 309–327.
- Fukuzawa, K.; Ikebata, W.; Sohmi, K. *J. Nutr. Sci. Vitaminol.* **1993**, *39*, 9–22.
- Barclay, L. R. C.; Baskin, K. A.; Dakin, K. A.; Locke, S. J.; Vinquist, M. R. *Can. J. Chem.* **1990**, *68*, 2258–2269.
- Eldho, N. V.; Feller, S. E.; Tristram-Nagle, S.; Polozov, I. V.; Gawrisch, K. *J. Am. Chem. Soc.* **2003**, *125*, 6409–6421.
- Huster, D.; Arnold, K.; Gawrisch, K. *J. Phys. Chem. B* **1999**, *103*, 243–251.
- Huster, D.; Gawrisch, K. *J. Am. Chem. Soc.* **1999**, *121*, 1992–1993.
- Soubias, O.; Gawrisch, K. *J. Am. Chem. Soc.* **2007**, *129*, 6678–6679.
- Wang, X.-H.; Ushio, H.; Ohshima, T. *Lipids* **2003**, *38*, 65–72.
- Lucas, R.; Comelles, F.; Alcántara, D.; Maldonado, O. S.; Curcuroze, M.; Parra, J. L.; Morales, J. C. *J. Agric. Food Chem.* **2010**, *58*, 8021–8026.
- Panya, A.; Laguerre, M.; Bayrasy, C.; Lecomte, J.; Villeneuve, P.; McClements, D. J.; Decker, E. A. *J. Agric. Food Chem.* **2012**, *60*, 2692–2700.
- Niki, E. *Free Radical Biol. Med.* **2009**, *47*, 469–484.
- Jomova, K.; Valko, M. *Toxicology* **2011**, *283*, 65–87.
- Genestra, M. *Cellular Signalling* **2007**, *19*, 1807–1819.
- Valko, M.; Leibfritz, D.; Moncol, J.; Cronin, M. T.; Mazur, M.; Telsler, J. *Int. J. Biochem. Cell Biol.* **2007**, *39*, 44–84.
- Droge, W. *Physiol. Rev.* **2002**, *82*, 47–95.

- (58) Pham-Huy, L. A.; He, H.; Huy, C. P. *Int. J. Biomed. Sci.* **2008**, *4*, 89–96.
- (59) Nelson, M. J.; Cowling, R. A.; Seitzl, S. P. *Biochemistry* **1994**, *33*, 4966–4973.
- (60) Cadenas, E.; Sies, H. *Free Radical Res.* **1998**, *28*, 601–609.
- (61) Tieleman, D. P.; Sansom, M. S. P.; acr C. Berendsen, H. J. *Biophys. J.* **1999**, *76*, 40–49.
- (62) Gu, F.; Netscher, T.; Atkinson, J. J. *Labelled Compd. Radiopharm.* **2006**, *49*, 733–743.
- (63) Müller, R. K.; Schneider, H. (Roche Vitamins Inc.). U.S. Patent 6066731, 2000.
- (64) Davis, J. H.; Jeffrey, K. R.; Bloom, M.; Valic, M. I.; Higgs, T. P. *Chem. Phys. Lett.* **1976**, *42*, 390–394.
- (65) Soni, S. P.; Ward, J. A.; Sen, S. E.; Feller, S. E.; Wassall, S. R. *Biochemistry* **2009**, *48*, 11097–11107.